ORIGINAL ARTICLE
UDC 519.6
https://doi.org/10.26907/2541-7746.2025.4.607-626

Numerical study of the 2D Sivashinsky equation for binary alloy solidification problems

R. Abazari[1] ✉, **K. Yildirim**[2]

[1]*Department of Mathematics, University of Mohaghegh Ardabili, Ardabil, Iran*

[2]*Muş Alparslan University, Muş, Turkey*

✉ *abazari-r@uma.ac.ir*

Abstract

Binary alloy solidification involves the transition of a liquid mixture of two metals into a solid phase and presents several complex challenges that researchers aim to address. These problems can be categorized into issues related to thermodynamics, diffusion, and macro- and microstructural evolution during the cooling process. The Sivashinsky equation is a fourth-order nonlinear partial differential equation that arises in the mathematical modeling of binary alloy solidification problems. In this article, we apply the Fourier spectral method combined with the Euler method to numerically solve the 2D Sivashinsky equation with periodic boundary conditions. A numerical study of the Sivashinsky equation is important because its analytical solution does not exist, except for trivial solutions. The error estimation of the approximate solution is provided. Furthermore, we show, both theoretically and numerically, that the proposed method preserves the decreasing mass condition of the obtained numerical solutions. Finally, to validate the theoretical results, three examples with different initial conditions are investigated.

Keywords: Sivashinsky equation, alloy solidification, Fourier spectral method, Euler method, mass conservation

For citation: Abazari R., Yildirim K. Numerical study of the 2D Sivashinsky equation for binary alloy solidification problems. *Uchenye Zapiski Kazanskogo Universiteta. Seriya Fiziko-Matematicheskie Nauki*, 2025, vol. 167, no. 4, pp. 607–626. https://doi.org/10.26907/2541-7746.2025.4.607-626.

ОРИГИНАЛЬНАЯ СТАТЬЯ
УДК 519.6
https://doi.org/10.26907/2541-7746.2025.4.607-626

Численное исследование двумерного уравнения Сивашинского для задач затвердевания бинарных сплавов

Р. Абазари[1] ✉, **К. Йилдирим**[2]

[1] *Кафедра математики, Университет Мохагеха Ардебили, г. Ардебиль, Иран*

[2] *Университет Муш Альпарслан, г. Муш, Турция*

✉ *abazari-r@uma.ac.ir*

Аннотация

Затвердевание бинарных сплавов представляет собой фазовый переход смеси двух металлов из жидкого состояния в твердое с образованием бикомпонентного материала. Изучение данного процесса связано с решением ряда сложных задач, являющихся предметом многих современных исследований в области термодинамики, диффузионного переноса, а также изменения макро- и микроструктуры веществ при охлаждении. Для математического описания затвердевания бинарных сплавов используется уравнение Сивашинского, которое относится к нелинейным дифференциальным уравнениям четвертого порядка в частных производных. Настоящая статья посвящена решению двумерного уравнения Сивашинского с периодическими граничными условиями методом Эйлера – Фурье. Численное исследование этого уравнения имеет особую значимость, поскольку его аналитические решения возможны только для простейших, тривиальных случаев. Проведена оценка погрешности приближенного решения. Кроме того, результаты теоретического анализа и численных экспериментов показали, что предложенный метод обеспечивает уменьшение массы для всех вычисленных решений. Рассмотрены три примера с различными начальными условиями.

Ключевые слова: уравнение Сивашинского, затвердевание сплавов, спектральный метод Фурье, метод Эйлера, сохранение массы

Для цитирования: *Abazari R., Yildirim K.* Numerical study of the 2D Sivashinsky equation for binary alloy solidification problems // Учен. зап. Казан. ун-та. Сер. Физ.-матем. науки. 2025. Т. 167, кн. 4. С. 607–626. https://doi.org/10.26907/2541-7746.2025.4.607-626.

1. Introduction

Binary alloy solidification is a non-equilibrium thermodynamic process of phase transformation in which a homogeneous liquid mixture of two elements cools and transitions into a solid with crystalline microstructure. The final solid morphology is determined by the interplay between thermal diffusion, solute redistribution, and capillary forces

at the solid–liquid interface. As the solid phase grows, solute atoms are typically rejected (for most phase diagrams), leading to composition gradients in the liquid that can cause instabilities and complex patterns such as dendritic structures. A good understanding of the solidification dynamics, including constitutional undercooling and the Mullins–Sekerka instability [1], is critical for predicting and tailoring properties like strength, corrosion resistance, and ductility in cast metals and engineered components [3, 4]. It is also important that solute diffusion along temperature gradients can induce a compositional segregation behavior, affecting the final alloy properties [5]. Advanced modeling techniques, including phase-field models and cellular automata, have been developed to simulate these processes more accurately [2]. Effective control of the solidification dynamics is essential for optimizing the mechanical performance of binary alloys in various applications. Fig. 1, (a)–(d) is a typical image sequence showing the progressive nucleation and growth of AI–Cu alloys inoculated with TiB_2 particles [6]. The mathematical modeling of alloy solidification problems is based on a nonlinear evolution equation known as the Sivashinsky equation, first formulated by G.I. Sivashinsky to describe minor thermal diffusive instabilities in laminar flame fronts and slight perturbations from a baseline Poiseuille flow in a film layer on an inclined plane in higher spatial dimensions [7, 8]. The Sivashinsky equation in two dimensions takes the following form [9]:

$$\begin{cases} u_t + \Delta^2 u + \alpha u = \Delta f(u), & \text{in } \Omega \times (0, T], \\ u = \Delta u = 0, & \text{on } \partial\Omega, \\ u(\mathbf{x}, 0) = u_0(\mathbf{x}), & \text{in } \bar{\Omega}, \end{cases} \tag{1}$$

where $f(u) = \frac{1}{2}u^2 - 2u$, Δ is the Laplacian operator, $\Omega = [0, L]^2 \subset \mathbb{R}^2$, and α is a positive constant. The Sivashinsky equation is also used to model the Bénard convection in an elongated box, long waves at the interface between two viscous fluids, and unstable drift waves in plasmas [8]. It belongs to the family of equations describing phase separation problems and shows a competition between destabilizing $(-\nabla^2 u)$ and stabilizing $(\nabla^4 u)$ forces, wich is mediated by a nonlinear term that generates a complex pattern-forming behavior. The main feature of the Sivashinsky equation (1) is the decrease of mass condition of its solution within the time domain [7–9], i.e.,

$$\int_\Omega u(., t)d\Omega \leq \int_\Omega u(., 0)d\Omega, \quad t > 0. \tag{2}$$

It can be concluded that the conservation of mass condition, $\int_\Omega u(., t)d\Omega = 0$, is satisfied in the steady state.

To date, studies on the one-dimensional (1D) and two-dimensional (2D) Sivashinsky equations remain quite rare. In [10], a splitting scheme based on the Crank–Nicolson method was proposed for the 1D Sivashinsky equation. Omrani developed a semi-implicit splitting finite-difference method to approximate the numerical solutions of the 1D Sivashinsky equation [12] and subsequently solved the same equation numerically using a linearized finite-difference method in [13]. Benammous et al. [14] applied a finite element method with an error estimate for the 1D Sivashinsky equation. In [15], Omrani introduced a piecewise linear semi-discrete finite element scheme to approximate the solutions of the 2D Sivashinsky equation (1). A linearized three-level difference method was employed by Rouis and Omrani to solve the 2D Sivashinsky equation in [16]. Ilati and Dehghan formulated a meshless weak form method based on the radial point interpolation technique for the Sivashinsky equation arising in the alloy solidification problem [11].

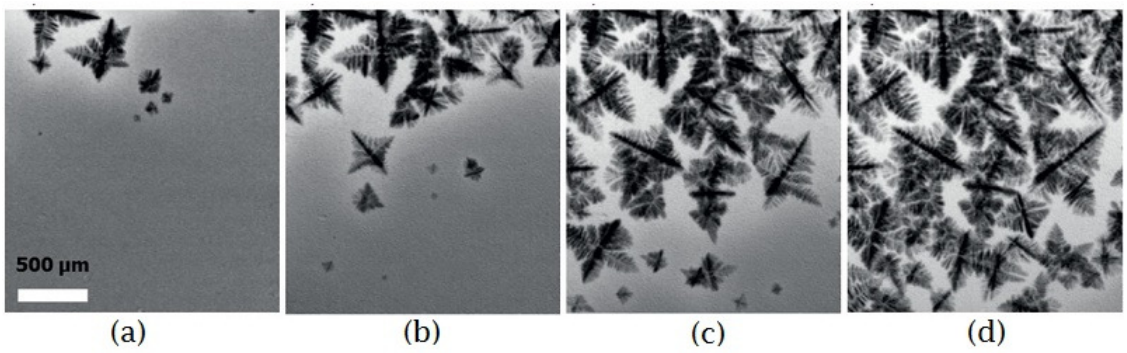

Fig. 1. Image sequence (a)–(d) illustrating the crystallization of solidifying Al–Cu alloys inoculated with TiB_2 particles [6]

Spectral methods are a class of numerical techniques for solving differential equations by expanding the solution in terms of globally defined basis functions, including orthogonal polynomials [19], Fourier series [20], wavelets [21], etc. These methods leverage the properties of these basis functions to achieve high accuracy with fewer degrees of freedom compared to traditional finite difference or finite element methods. Spectral methods are particularly effective for problems with smooth solutions, as they can capture details of the solution with exponential convergence rates. They are widely used in various fields, such as fluid dynamics, meteorology, and computational physics, to facilitate the modeling of complex systems.

In this article, the Fourier spectral method combined with the Euler scheme was applied to approximate the numerical solution of the 2D Sivashinsky equation (1), as a mathematical modeling of binary alloy solidification problems, under the periodic boundary condition. With this aim, a limited set of trigonometric fundamental functions were used as trail functions for the Fourier spectral method and then merged in a linear manner to find a numerical solution of equation (1). Finally, the Euler method was utilized to solve the reduced equation. The selected trail functions were as smooth as possible. Since the Fourier spectral method represents the obtained numerical solutions on a discrete set of grid points, it reduces the computational cost associated with evaluating higher dimensions of the differentiating terms of the Sivashinsky equation (1). The proposed method preserves the decreasing mass condition of the obtained numerical solutions.

2. Numerical Simulation

In this section, we propose a scheme based on the Fourier spectral method and the forward Euler method for solving the 2D Sivashinsky equation (1). Let N_x, N_y be positive integers and $h_x = \dfrac{L}{N_x}, h_y = \dfrac{L}{N_y}$ be the step sizes of the x- and y-directions, respectively, with $\tau = \dfrac{T}{N_t}$ set as the time step size. Suppose that $u^k_{m,n}$ is an approximation of $u(x_m, y_n, t_k)$, where $x_m = mh_x$, $m = 0, 1, 2, \ldots, N_x$, $y_n = nh_y$, $n = 0, 1, 2, \ldots, N_y$ and $t_k = k\tau$, $k = 0, 1, 2, \ldots, N_t$ are the grid points. Here, the superscripts m, n denote a quantity associated with the special domain mesh points x_m, y_n, while the subscript n refers to a quantity associated with the time level t_n.

Let $S^\tau_{h_x,h_y} = \left\{u^k_{m,n} | m = 0, 1, 2, \ldots, N_x \ \& \ n = 0, 1, 2, \ldots, N_y \ \& \ k = 0, 1, \ldots, N_t\right\}$ be a desired approximate solution. For any $u, v \in S^\tau_{h_x,h_y}$ by $(.,.)_{h_x,h_y}$, the discrete L^2 inner product $(.,.)_{h_x,h_y}$ is defined as follows:

$$(u^k, v^k)_{h_x,h_y} = h_x h_y \sum_{m=0}^{N_x} \sum_{n=0}^{N_y} u^k_{m,n} v^k_{m,n}. \tag{3}$$

The discrete L^2 norm is denoted by $||.||$ and written as

$$||u^k||^2 = (u^k, u^k)_{h_x,h_y}. \tag{4}$$

Under the above assumption, the discrete Fourier transform of $u^k_{m,n}$ and its inverse transform are

$$\hat{u}^k_{p,q} = \sum_{m=0}^{N_x-1} \sum_{n=0}^{N_y-1} u^k_{m,n} e^{i(\xi_p x_m + \eta_q y_n)} \tag{5}$$

and

$$u^k_{m,n} = \frac{1}{N_x N_y} \sum_{p=0}^{N_x-1} \sum_{q=0}^{N_y-1} \hat{u}^k_{p,q} e^{i(\xi_p x_m + \eta_q y_n)}, \tag{6}$$

where $\xi_p = \dfrac{2\pi p}{L}$ and $\eta_q = \dfrac{2\pi q}{L}$. To develop an implicit-explicit Euler method for (1), we treat the terms $\Delta^2 u + 2\Delta u + \alpha u$ implicitly and the right-hand term $\dfrac{1}{2}\Delta u^2$ explicitly, which results in

$$\frac{u^k - u^{k-1}}{\tau} + \Delta^2 u^k + 2\Delta u^k + \alpha u^k = \frac{1}{2}\Delta (u^{k-1})^2 + R^k, \tag{7}$$

where $|R^k| < c\tau$ and c is a constant. Multiplying both sides of (7) by τ and neglecting the small term τR^k, we arrive at

$$(1 + \alpha\tau)u^k + \tau\Delta^2 u^k + 2\tau\Delta u^k = u^{k-1} + \frac{\tau}{2}\Delta (u^{k-1})^2 + \tau R^k. \tag{8}$$

Since the time step size τ and the error term R^k are small, then its multiplying can be eliminated from (8). Consequently, the time discrete scheme for equation (1) yields to

$$(1 + \alpha\tau)u^k + \tau\Delta^2 u^k + 2\tau\Delta u^k = u^{k-1} + \frac{\tau}{2}\Delta (u^{k-1})^2. \tag{9}$$

Applying the Fourier transform to equation (9), we get

$$(1 + \alpha\tau)\hat{u}^k_{pq} + \tau(\xi_p^2 + \eta_q^2)^2 \hat{u}^k_{pq} - 2\tau(\xi_p^2 + \eta_q^2)\hat{u}^k_{pq} = \hat{u}^{k-1}_{pq} - \frac{\tau}{2}(\xi_p^2 + \eta_q^2)(\hat{u}^{k-1}_{pq})^2, \tag{10}$$

which simplifies to

$$\hat{u}^k_{pq} = \frac{\hat{u}^{k-1}_{pq} - \frac{\tau}{2}(\xi_p^2 + \eta_q^2)(\hat{u}^{k-1}_{pq})^2}{1 + \alpha\tau - 2\tau(\xi_p^2 + \eta_q^2) + \tau(\xi_p^2 + \eta_q^2)^2}. \tag{11}$$

Using equation (11), an approximate solution can be obtained by recovering u^k_{mn} from $\hat{u}^k_{pq}$.

In the next subsection, we demonstrate the stability of the proposed spectral method (9) in the L^2 norm and investigate its convergence.

2.1. Stability and convergence analysis. Consider the space of $L^2(\Omega)$ as the Lebesgue space with the following inner product and related L^2 norm:

$$(u,v)=\int_\Omega uvd\Omega,\quad \|v\|_{L^2}=(v,v)^{\frac{1}{2}}\qquad \forall u,v\in L^2(\Omega).$$

To analyze the stability and convergence of difference scheme (9), we employ the energy method. For this purpose, we introduce the following spaces:

$$H^2(\Omega)=\left\{v: v\in L^2(\Omega),\nabla.v\in L^2(\Omega)\right\},$$
$$H_0^2(\Omega)=\left\{v\in H^2(\Omega): v|_{\partial\Omega}=0,\frac{\partial v}{\partial n}\Big|_{\partial\Omega}=0\right\}.$$

Theorem 1. *Let $u^k\in H_0^2(\Omega)$. Then the implicit-explicit Euler scheme defined in (9) is stable in the L^2 norm.*

Proof. The proof follows a strategy similar to that of [10,18]. Let u^k and U^k be the exact and approximate solutions of equation (1), respectively, and $e^k=u^k-U^k$ be the error between them. Then the roundoff error of the implicit-explicit Euler scheme (9) takes the form

$$(1+\alpha\tau)e^k+2\tau\Delta e^k+\tau\Delta^2e^k=e^{k-1}+\frac{\tau}{2}\Delta\left(\left(u^{k-1}\right)^2-\left(U^{k-1}\right)^2\right). \tag{12}$$

Pairing equation (12) with e^k and integrating on Ω, we get

$$(1+\alpha\tau)\left(e^k,e^k\right)+2\tau\left(\Delta e^k,e^k\right)+\tau\left(\Delta^2e^k,e^k\right)=\left(e^{k-1},e^k\right)+\frac{\tau}{2}\left(\Delta\left(\left(u^{k-1}\right)^2-\left(U^{k-1}\right)^2\right),e^k\right). \tag{13}$$

Via two consecutive integrations by part of the term (Δ^2e^k,e^k) on Ω, we obtain

$$\begin{aligned}\left(\Delta^2e^k,e^k\right)&=\left(\frac{\partial}{\partial k}\left(\Delta e^k\right),e^k\right)_{\partial\Omega}-\left(\nabla\Delta e^k,\nabla e^k\right)\\&=\left(\frac{\partial}{\partial k}\left(\Delta e^k\right),e^k\right)_{\partial\Omega}-\left(\Delta e^k,\frac{\partial e^k}{\partial k}\right)_{\partial\Omega}+\left(\Delta e^k,\Delta e^k\right).\end{aligned} \tag{14}$$

From the boundary conditions of the Sivashinsky equation (1), $u|_{\partial\Omega}=\Delta u|_{\partial\Omega}=0$, we have $\left(\frac{\partial}{\partial k}\left(\Delta e^k\right),e^k\right)_{\partial\Omega}=\left(\Delta e^k,\frac{\partial e^k}{\partial k}\right)_{\partial\Omega}=0$, and, since $e^k\in H_0^2(\Omega)$, it is concluded that $\left(\Delta^2e^k,e^k\right)=\left(\Delta e^k,\Delta e^k\right)$. Then equation (13) can be rewritten as

$$(1+\alpha\tau)\left(e^k,e^k\right)+2\tau\left(\Delta e^k,e^k\right)+\tau\left(\Delta e^k,\Delta e^k\right)=\left(e^{k-1},e^k\right)+\frac{\tau}{2}\left(\Delta\left(\left(u^{k-1}\right)^2-\left(U^{k-1}\right)^2\right),e^k\right). \tag{15}$$

Applying the Schwarz inequality to equation (15) yields

$$\begin{aligned}&(1+(\alpha+1)\tau)\left\|e^k\right\|^2_{L^2(\Omega)}+\frac{7\tau}{4}\|\Delta e^k\|^2_{L^2(\Omega)}\\&\le\frac{1}{2}\|e^{k-1}\|^2_{L^2(\Omega)}+\frac{1}{2}\|e^k\|^2_{L^2(\Omega)}+\frac{\tau}{4}\|(u^{k-1})^2-(U^{k-1})^2\|^2_{L^2(\Omega)}.\end{aligned} \tag{16}$$

The term $\|(u^{k-1})^2-(U^{k-1})^2\|^2_{L^2(\Omega)}$ satisfies the Lipschitz condition

$$\begin{aligned}|(u^{k-1})^2-(U^{k-1})^2| &\le |u^{k-1}-U^{k-1}||u^{k-1}+U^{k-1}|\\ &\le \frac{1}{2}M^*|u^{k-1}-U^{k-1}|\\ &\le \mathcal{L}|u^{k-1}-U^{k-1}|,\end{aligned} \tag{17}$$

where $M^* \ge \max_{u\in C^\infty(\Omega)}|u|$ and $\mathcal{L}$ is the Lipschitz condition. Consequently, inequality (16) becomes

$$\left(\frac{1}{2}+(\alpha+1)\tau\right)\|e^k\|^2_{L^2(\Omega)}+\frac{7\tau}{4}\|\Delta e^k\|^2_{L^2(\Omega)} \le \left(\frac{1}{2}+\frac{\tau\mathcal{L}^2}{4}\right)\|e^{k-1}\|^2_{L^2(\Omega)}. \tag{18}$$

After the simplification step, we have

$$\begin{aligned}\|e^k\|^2_{L^2(\Omega)} &\le \left(\frac{\frac{1}{2}+\frac{\tau\mathcal{L}^2}{4}}{\frac{1}{2}+(\alpha+1)\tau}\right)\|e^{k-1}\|^2_{L^2(\Omega)} \le \left(\frac{\frac{1}{2}+\frac{\tau\mathcal{L}^2}{4}}{\frac{1}{2}+(\alpha+1)\tau}\right)^2\|e^{k-1}\|^2_{L^2(\Omega)}\\ &\le \cdots \le \left(\frac{\frac{1}{2}+\frac{\tau\mathcal{L}^2}{4}}{\frac{1}{2}+(\alpha+1)\tau}\right)^k\|e^0\|^2_{L^2(\Omega)}, \quad k=1,2,\ldots,N.\end{aligned} \tag{19}$$

To derive a relation between $\|e^k\|$ and $\|e^0\|$ independent of τ, we have

$$\lim_{k\to\infty}\left(\frac{\frac{1}{2}+\frac{\tau\mathcal{L}^2}{4}}{\frac{1}{2}+(\alpha+1)\tau}\right)^k = \lim_{k\to\infty}\left(\frac{1+\frac{T\mathcal{L}^2}{2k}}{1+\frac{2(\alpha+1)T}{k}}\right)^k = e^{T\left(\frac{\mathcal{L}^2}{2}-2(\alpha+1)\right)}.$$

Therefore,

$$\|e^k\|^2_{L^2(\Omega)} \le ce^{T\left(\frac{\mathcal{L}^2}{2}-2(\alpha+1)\right)}\|e^0\|^2_{L^2(\Omega)}, \quad k=1,2,\ldots,N,$$

where c is a positive constant. By setting $C=ce^{T\left(\frac{\mathcal{L}^2}{2}-2(\alpha+1)\right)}$, we get

$$\|e^k\|^2_{L^2(\Omega)} \le C\|e^0\|^2_{L^2(\Omega)}, \quad k=1,2,\ldots,N.$$

This completes the proof. □

Remark 1. From the result of Theorem 1, it can be concluded that

If $\frac{\mathcal{L}^2}{2}-2(\alpha+1)<0$, then the scheme defined in (9) exhibits strong stability.
If $\frac{\mathcal{L}^2}{2}-2(\alpha+1)>0$, then the scheme defined in (9) exhibits weak stability.
If $\frac{\mathcal{L}^2}{2}-2(\alpha+1)=0$, then the scheme defined in (9) exhibits strong stability.

Remark 2. Although it must be that $\alpha>0$, if $\alpha=0$, then, from the result of Theorem 1, it is concluded that $\mathcal{L}<2$ for strong stability of the scheme defined in (9).

In the next theorem, the convergence of the proposed method is investigated.

Theorem 2. *Let $u^k \in H_0^2(\Omega)$. Then the time discrete solution obtained by the proposed scheme defined in* (9) *is L^2-convergent with the convergence order $O(\tau)$.*

Proof. The proof proceeds analogously to that of [10, 18]. Let u^k and U^k be the exact and approximate solutions of the Sivashinsky equation (1), respectively, and $\rho^k = u^k - U^k$. Substituting ρ^k in difference scheme (9), we have

$$(1+\alpha\tau)\rho^k + 2\tau\Delta\rho^k + \tau\Delta^2\rho^k = \rho^{k-1} + \frac{\tau}{2}\Delta\left(\left(u^{k-1}\right)^2 - \left(U^{k-1}\right)^2\right) + \tau R^k, \tag{20}$$

where $|R^k| < C\tau$ for a positive constant C and $\rho^0 = 0$. Multiplying equation (20) by ρ^k and integrating on Ω, we get

$$\begin{aligned}&(1+\alpha\tau)\big(\rho^k,\rho^k\big) + 2\tau\big(\Delta\rho^k,\rho^k\big) + \tau\big(\Delta\rho^k,\Delta\rho^k\big)\\ &= \big(\rho^{k-1},\rho^k\big) + \frac{\tau}{2}\left(\left(u^{k-1}\right)^2 - \left(U^{k-1}\right)^2,\Delta\rho^k\right) + \tau\big(R^k,\rho^k\big).\end{aligned} \tag{21}$$

Applying the Schwarz inequality to equation (21) leads to

$$\begin{aligned}&\left(\frac{1}{2} + (\alpha+\frac{1}{2})\tau\right)\|\rho^k\|^2_{L^2(\Omega)} + \frac{7\tau}{4}\|\Delta\rho^k\|^2_{L^2(\Omega)}\\ &\le \frac{1}{2}\|\rho^{k-1}\|^2_{L^2(\Omega)} + \frac{\tau}{4}\|\left(u^{k-1}\right)^2 - \left(U^{k-1}\right)^2\|^2_{L^2(\Omega)} + \frac{\tau}{2}\|R^k\|^2_{L^2(\Omega)}.\end{aligned} \tag{22}$$

The term $\|(u^{k-1})^2 - (U^{k-1})^2\|^2_{L^2(\Omega)}$ satisfies the Lipschitz condition as

$$\|(u^{k-1})^2 - (U^{k-1})^2\|^2_{L^2(\Omega)} \le \mathcal{L}^2\|\rho^{k-1}\|^2_{L^2(\Omega)},$$

and inequality (22) leads to

$$\left(\frac{1}{2} + (\alpha+\frac{1}{2})\tau\right)\|\rho^k\|^2_{L^2(\Omega)} + \frac{7\tau}{4}\|\Delta\rho^k\|^2_{L^2(\Omega)} \le \left(\frac{1}{2} + \frac{\tau\mathcal{L}^2}{4}\right)\|\rho^{k-1}\|^2_{L^2(\Omega)} + \frac{\tau}{2}\|R^k\|^2_{L^2(\Omega)}. \tag{23}$$

Neglecting the term $\|\Delta\rho^k\|$ and considering that $\left(\frac{1}{2}+\frac{\tau}{2}\right) < \left(\frac{1}{2}+(\alpha+\frac{1}{2})\tau\right)$, we can rewrite inequality (23) as follows:

$$\left(\frac{1}{2} + \frac{\tau}{2}\right)\|\rho^k\|^2_{L^2(\Omega)} \le \left(\frac{1}{2} + \frac{\tau\mathcal{L}^2}{4}\right)\|\rho^{k-1}\|^2_{L^2(\Omega)} + \tau\left(\frac{1}{2} + \frac{\tau\mathcal{L}^2}{4}\right)\|R^k\|^2_{L^2(\Omega)}. \tag{24}$$

Considering relation (24) for $k-1, k-2, \ldots, 1, 0$, we get

$$\begin{aligned}\|\rho^k\|^2_{L^2(\Omega)} &\le \left(\frac{\frac{1}{2}+\frac{\tau\mathcal{L}^2}{4}}{\frac{1}{2}+\frac{\tau}{2}}\right)\|\rho^{k-1}\|^2_{L^2(\Omega)} + \tau\left(\frac{\frac{1}{2}+\frac{\tau\mathcal{L}^2}{4}}{\frac{1}{2}+\frac{\tau}{2}}\right)\|R^k\|^2_{L^2(\Omega)}\\ &\le \left(\frac{\frac{1}{2}+\frac{\tau\mathcal{L}^2}{4}}{\frac{1}{2}+\frac{\tau}{2}}\right)^2\|\rho^{k-2}\|^2_{L^2(\Omega)} + \tau\left(\frac{\frac{1}{2}+\frac{\tau\mathcal{L}^2}{4}}{\frac{1}{2}+\frac{\tau}{2}}\right)^2\|R^{k-1}\|^2_{L^2(\Omega)} + \tau\left(\frac{\frac{1}{2}+\frac{\tau\mathcal{L}^2}{4}}{\frac{1}{2}+\frac{\tau}{2}}\right)\|R^k\|^2_{L^2(\Omega)}\\ &\le \cdots \le \left(\frac{\frac{1}{2}+\frac{\tau\mathcal{L}^2}{4}}{\frac{1}{2}+\frac{\tau}{2}}\right)^k\|\rho^0\|^2_{L^2(\Omega)} + \tau\sum_{j=1}^{k}\left(\frac{\frac{1}{2}+\frac{\tau\mathcal{L}^2}{4}}{\frac{1}{2}+\frac{\tau}{2}}\right)^j\|R^{k-j+1}\|^2_{L^2(\Omega)}, \quad k = 1,2,\ldots,N.\end{aligned} \tag{25}$$

Since $\rho = 0$ and $|R^k| < C\tau$, we have

$$\|\rho^k\|^2_{L^2(\Omega)} \leq \tau \sum_{j=1}^{k} \left(\frac{\frac{1}{2}+\frac{\tau\mathcal{L}^2}{4}}{\frac{1}{2}+\frac{\tau}{2}} \right)^j \|R^{k-j+1}\|^2_{L^2(\Omega)} \leq k\tau \left(\frac{\frac{1}{2}+\frac{\tau\mathcal{L}^2}{4}}{\frac{1}{2}+\frac{\tau}{2}} \right)^k C^2\tau^2. \tag{26}$$

In addition,

$$\lim_{k\to\infty} \left(\frac{\frac{1}{2}+\frac{\tau\mathcal{L}^2}{4}}{\frac{1}{2}+\frac{\tau}{2}} \right)^k = \lim_{k\to\infty} \left(\frac{1+\frac{T\mathcal{L}^2}{2k}}{1+\frac{T}{k}} \right)^k = e^{\frac{T}{2}(\mathcal{L}^2-2)}.$$

Then we obtain

$$\|\rho^k\|^2_{L^2(\Omega)} \leq Te^{\frac{T}{2}(\mathcal{L}^2-2)}C^2\tau^2.$$

Setting $\mathcal{C} = \sqrt{TC^2e^{\frac{T}{2}(\mathcal{L}^2-2)}}$, we get

$$\|\rho^k\|^2_{L^2(\Omega)} \leq \mathcal{C}\tau,$$

which shows that the implicit-explicit Euler scheme defined in (9) is L^2-convergent with the convergence order $O(\tau)$. This completes the proof. □

3. Mass-Decreasing Property

This section demonstrates that the proposed approach confirms the mass-decreasing property (2) of the Sivashinsky equation (1). Using the same reasoning as in [17, 18], a similar conclusion can be reached. With this aim, we take the inner product of equation (12) with a constant grid function $\mathbf{1}$ and get that

$$\begin{aligned} &\left(u^k, \mathbf{1}\right)_{h_x,h_y} + \frac{\tau}{1+\alpha\tau}\left(\Delta^2 u^k, \mathbf{1}\right)_{h_x,h_y} + \frac{2\tau}{1+\alpha\tau}\left(\Delta u^k, \mathbf{1}\right)_{h_x,h_y} \\ &= \frac{1}{1+\alpha\tau}\left(u^{k-1}, \mathbf{1}\right)_{h_x,h_y} + \frac{\tau}{2(1+\alpha\tau)}\left(\Delta(u^{k-1})^2, \mathbf{1}\right)_{h_x,h_y}. \end{aligned} \tag{27}$$

Let us consider the boundary values (7)-(9), for $\left(\Delta u^k, \mathbf{1}\right)_{h_x,h_y}$, and have that

$$\begin{aligned} \left(\Delta u^k, \mathbf{1}\right)_{h_x,h_y} &= h_x h_y \sum_{m=1}^{N_x}\sum_{n=1}^{N_y} (\delta_x^2 + \delta_y^2) u^k_{m,n} \\ &= h_x h_y \sum_{m=1}^{N_x}\sum_{n=1}^{N_y} \left(\frac{\delta_x^+ u^k_{m,n} - \delta_x^+ u^k_{m-1,n}}{h_x} + \frac{\delta_y^+ u^k_{m,n} - \delta_y^+ u^k_{m,n-1}}{h_y} \right) \\ &= h_y \sum_{m=1}^{N_x} \left(\delta_x^+ u^k_{m,N_y} - \delta_x^+ u^k_{m-1,0} \right) + h_x \sum_{n=1}^{N_y} \left(\delta_y^+ u^k_{N_x,n} - \delta_y^+ u^k_{0,n-1} \right) = 0. \end{aligned} \tag{28}$$

Since $\left(\Delta^2 u^k, \mathbf{1}\right)_{h_x,h_y} = \left(\Delta u^k, \Delta\mathbf{1}\right)_{h_x,h_y} = \left(\Delta u^k, 0\right)_{h_x,h_y}$, then $\left(\Delta^2 u^k, \mathbf{1}\right)_{h_x,h_y} = 0$. Similarly, we have $\left(\Delta(u^{k-1})^2, \mathbf{1}\right)_{h_x,h_y} = 0$. By substitution of these values in equation (27), it is found that $\left(u^k, \mathbf{1}\right)_{h_x,h_y} = \frac{1}{1+\alpha\tau}\left(u^{k-1}, \mathbf{1}\right)_{h_x,h_y}$. Since α is a positive constant, the following theorem can be derived.

Theorem 3. *The mass of scheme (12) under the boundary conditions (7)–(9) satisfies the decreasing property, i.e.,*

$$\left(u^k, \mathbf{1}\right)_{h_x,h_y} \leq \left(u^{k-1}, \mathbf{1}\right)_{h_x,h_y} \qquad \forall k \geq 1.$$

4. Numerical Experiment

As mentioned in the Introduction, solidification represents a fundamental process in materials science that has a significant influence on the microstructure and properties of metals and alloys. Binary alloy solidification, which is the focus of this study and consists in the cooling and phase transformation of a mixture of two metallic elements from a liquid to a solid state, determines and can alter many functional properties of alloys, including their mechanical strength, thermal stability, corrosion resistance, etc.

During solidification, numerous processes take place, such as nucleation, dendritic growth, spinodal decomposition, solute partitioning, and microsegregation (coring). The dynamics of these processes depends on the cooling rates and alloy composition. Binary alloy solidification occurs naturally in metallurgy and even planetary science. In this section, three examples are shown, each with a different type of initial condition: benchmark cross initial value (as a toy model of alloy solidification), smooth initial value (a more realistic model of alloy solidification) [9], and random initial value (as a spinodal decomposition model), all presented in Fig. 2. The experiments were performed using Python 3.9.

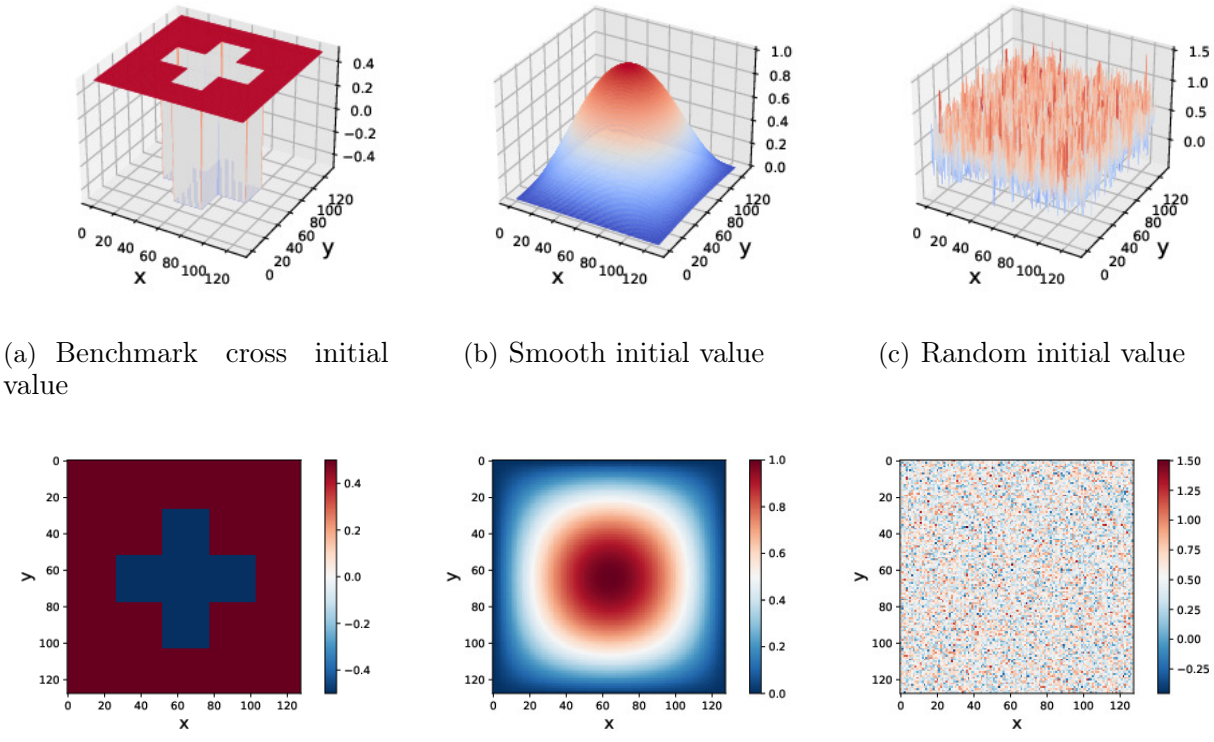

(a) Benchmark cross initial value (b) Smooth initial value (c) Random initial value

(d) Pseudo-color plot of (a) (e) Pseudo-color plot of (b) (f) Pseudo-color plot of (c)

Fig. 2. Initial values of (a) example 1, (b) example 2, and (c) example 3. Panels (d), (e), and (f) display the pseudo-color plots of (a), (b), and (c), respectively, on a uniform 128×128 mesh

The obtained numerical results for each of the three examples confirm that the proposed method satisfies the property of mass decreasing condition (2). In all examples, we set $\alpha = 1$ and we divide the domain $(0,1)^2$ into $N_x \times N_y$ meshgrid, where $N_x = N_y = N = \{8, 16, 32, 64, 128\}$ with the corresponding step size h_x and h_y in the x- and y-directions such that $h_x = h_y = h_d = \dfrac{1}{N(d)}$ for $d = 1, 2, 3, 4, 5$. In order to further assess the numerical results, the discrete L^2 error is estimated as a difference between the approximate solutions $u^k_{m,n}$ computed on two consecutive grids with the time grid $t_k = k\tau$ for $k = 0, 1, 2, \ldots, N_t$ as follows

$$\|.\|_2 = \left((h_d)^2 \sum_{m=1}^{N(d)} \sum_{n=1}^{N(d)} \left(u^{N_t,\tau}_{m,n} - u^{\frac{N_t}{2},2\tau}_{m,n} \right)^2 \right)^{\frac{1}{2}},$$

where $u^{N_t,\tau}_{m,n} = u^{N_t}_{m,n}$ is the numerical solution with the splitting time step size τ. Since no exact solution exists for the Sivashinsky equation (1), we can assess the convergence rate of the proposed approach by measuring the ratios of differences between the approximate solutions $u^k_{m,n}$ computed for different step sizes h_x and h_y. Most commonly, we compare solutions, where h_x and h_y are halved successively, then the convergence rate can be computed by the formula

$$\text{order} = \log_2 \left(\frac{||\mathbf{u}^{\frac{N}{2},2\tau} - \mathbf{u}^{\frac{N}{4},4\tau}||_2}{||\mathbf{u}^{N,\tau} - \mathbf{u}^{\frac{N}{2},2\tau}||_2} \right). \tag{29}$$

Most studies conducted on the 2D Sivashinsky equation have approached the problem from a theoretical perspective, and only a few of them report numerical results. To compare the numerical results of the proposed method and other similar methods, we consider examples 2 and 3 from [11], with the outcomes presented in Tables 1, 3, and 4. The numerical comparisons demonstrate a decrease in mass conservation of the proposed method as time increases, which is consistent with the statement of Theorem 3.

In light of the above, the following three examples are considered.

Example 1. In the first example, we consider the Sivashinsky equation (1) under the following benchmark cross initial value (Fig. 2, (a)):

$$\begin{aligned} u_0(x,y) = \frac{1}{2} &- \left(H\left(x - \frac{1}{5}\right) - H\left(x - \frac{4}{5}\right) \right) \left(H\left(y - \frac{2}{5}\right) - H\left(y - \frac{3}{5}\right) \right) \\ &- \left(H\left(x - \frac{2}{5}\right) - H\left(x - \frac{3}{5}\right) \right) \left(H\left(y - \frac{3}{5}\right) - H\left(y - \frac{4}{5}\right) \right) \\ &- \left(H\left(x - \frac{2}{5}\right) - H\left(x - \frac{3}{5}\right) \right) \left(H\left(y - \frac{1}{5}\right) - H\left(y - \frac{2}{5}\right) \right), \end{aligned} \tag{30}$$

where $(x, y) \in \Omega = [0, 1] \times [0, 1]$ and $H(x-.)$ and $H(y-.)$ are the Heaviside functions. Binary alloy solidification with a cross initial value is a common benchmark problem in computational materials science for testing solidification models and numerical methods. It describes the solidification of a binary alloy from a molten state with an initial composition profile shaped like a cross. The numerical solutions of the Sivashinsky equation (1) corresponding to initial condition (30) with step sizes $h = k = \dfrac{1}{128}$ and $\tau = \dfrac{4}{25}h$ at times $t = \{0.5, 3, 5, 10, 30, 50\}$ are shown in Fig. 3. According to Fig. 3, the solution loses its mass and tends to a steady state.

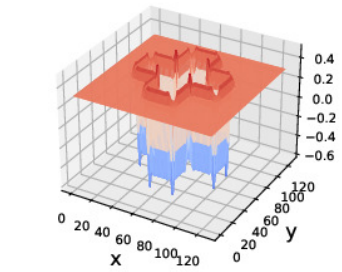

(a) $t = 0.5$

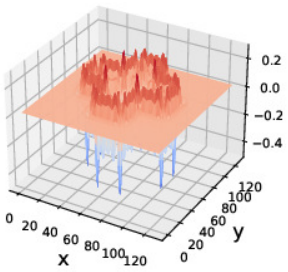

(b) $t = 3$

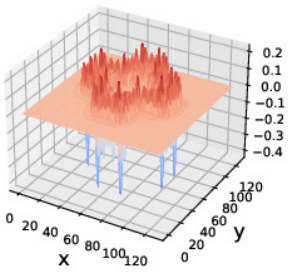

(c) $t = 5$

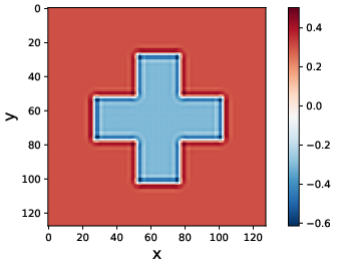

(d) Pseudo-color plot of (a)

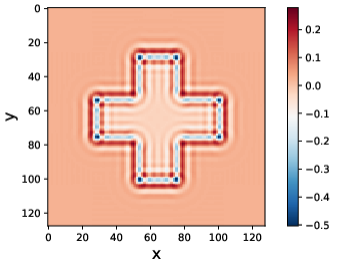

(e) Pseudo-color plot of (b)

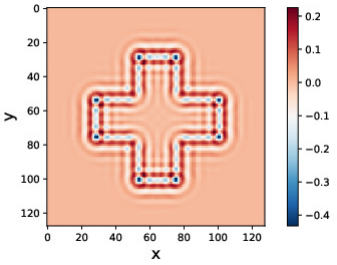

(f) Pseudo-color plot of (c)

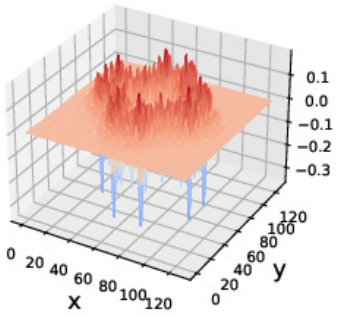

(g) $t = 10$

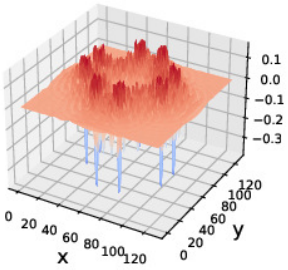

(h) $t = 30$

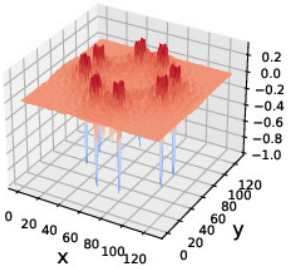

(i) $t = 50$

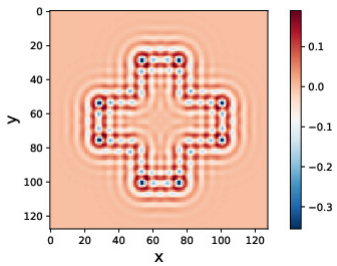

(j) Pseudo-color plot of (g)

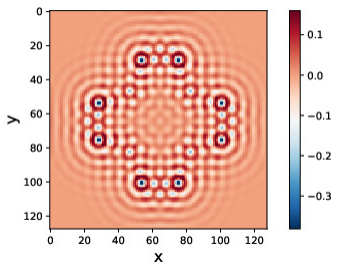

(k) Pseudo-color plot of (h)

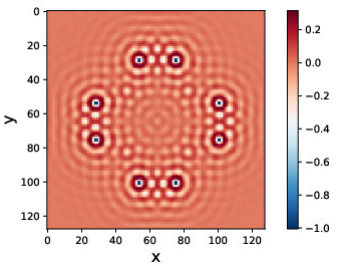

(l) Pseudo-color plot of (i)

Fig. 3. The first and third rows are the numerical solutions of example 1 with $h = k = \dfrac{1}{128}$ and $\tau = \dfrac{4}{25}h$ at times (a) t=0.5, (b) t=3, (c) t=5, (g) t=10, (h) t=30, and (i) t=50. The second and fourth rows are the pseudo-color plots of the first and third rows on a uniform 128×128 mesh

The L^2 error and convergence rate of the numerical solution of example 1 at times $t = 0.5, 1.5, 3, 5$ for $h = k = \left\{\frac{1}{16}, \frac{1}{32}, \frac{1}{64}, \frac{1}{128}\right\}$ and $\tau = \frac{4}{25}h$ are given in Table 1. The reduction in mass condition observed in the numerical solution of example 1 with initial values (30) is also illustrated in Fig. 4 (solid line).

Table 1. L^2 error of example 1 with $h = k = \frac{1}{N}$ and $\tau = \frac{4}{25}h$ at times $t = 0.5, 1.5, 3$ and $t = 5$

N	$t = 0.5$	order	$t = 1.5$	order	$t = 3$	order	$t = 5$	order
16	9.7076e-02	–	1.1125e-01	–	1.3685e-01	–	1.5663e-01	–
32	4.3349e-02	1.16	4.1864e-02	1.41	4.1988e-02	1.70	4.1432e-02	1.92
64	1.5336e-02	1.49	1.4496e-02	1.53	1.1330e-02	1.89	1.0504e-02	1.98
128	2.8300e-03	2.43	2.6352e-03	2.46	1.9485e-03	2.54	1.7573e-03	2.58

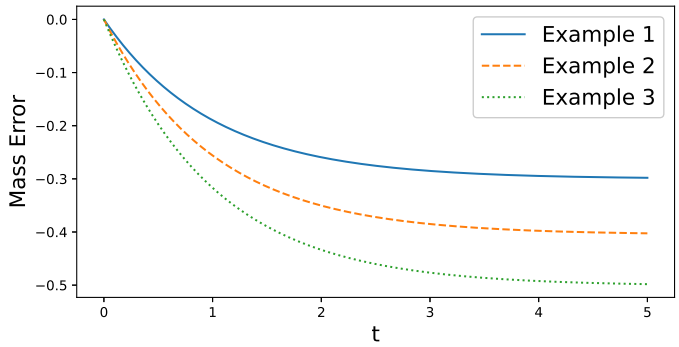

Fig. 4. Decrease in the mass error for the numerical solution of example 1 (solid line), example 2 (dashed line), and example 3 (dotted line) at $t = 0 : \frac{1}{128} : 5$ on a 128×128 mesh

Example 2. In the second example [9], the following smooth initial value is considered for the Sivashinsky equation (1)

$$u_0(x, y) = \sin(2\pi x)\sin(2\pi y), \quad (x, y) \in \Omega = [0, 1] \times [0, 1]. \tag{31}$$

Binary alloy solidification with smooth initial conditions is a fundamental problem in computational materials science for studying how smooth composition and temperature gradients evolve during solidification. This approach avoids discontinuities present in sharp interface benchmarks, making well-suited to diffuse-interface models like phase-field methods. The numerical profiles of this example with step sizes $h = k = \frac{1}{128}$ and $\tau = \frac{4}{25}h$ at times $t = \{0.5, 1.5, 3, 4, 5, 6\}$ are shown in Fig. 5.

The L_2 errors of the proposed numerical solution and the L_2 errors of the meshless global weak form method under the same initial condition (31) with $\tau = 0.001$ at $t = 1$ is shown in Table 2. The numerical results of this example agree with those discussed in [11] for the same example using the meshless method based on the radial point interpolation technique.

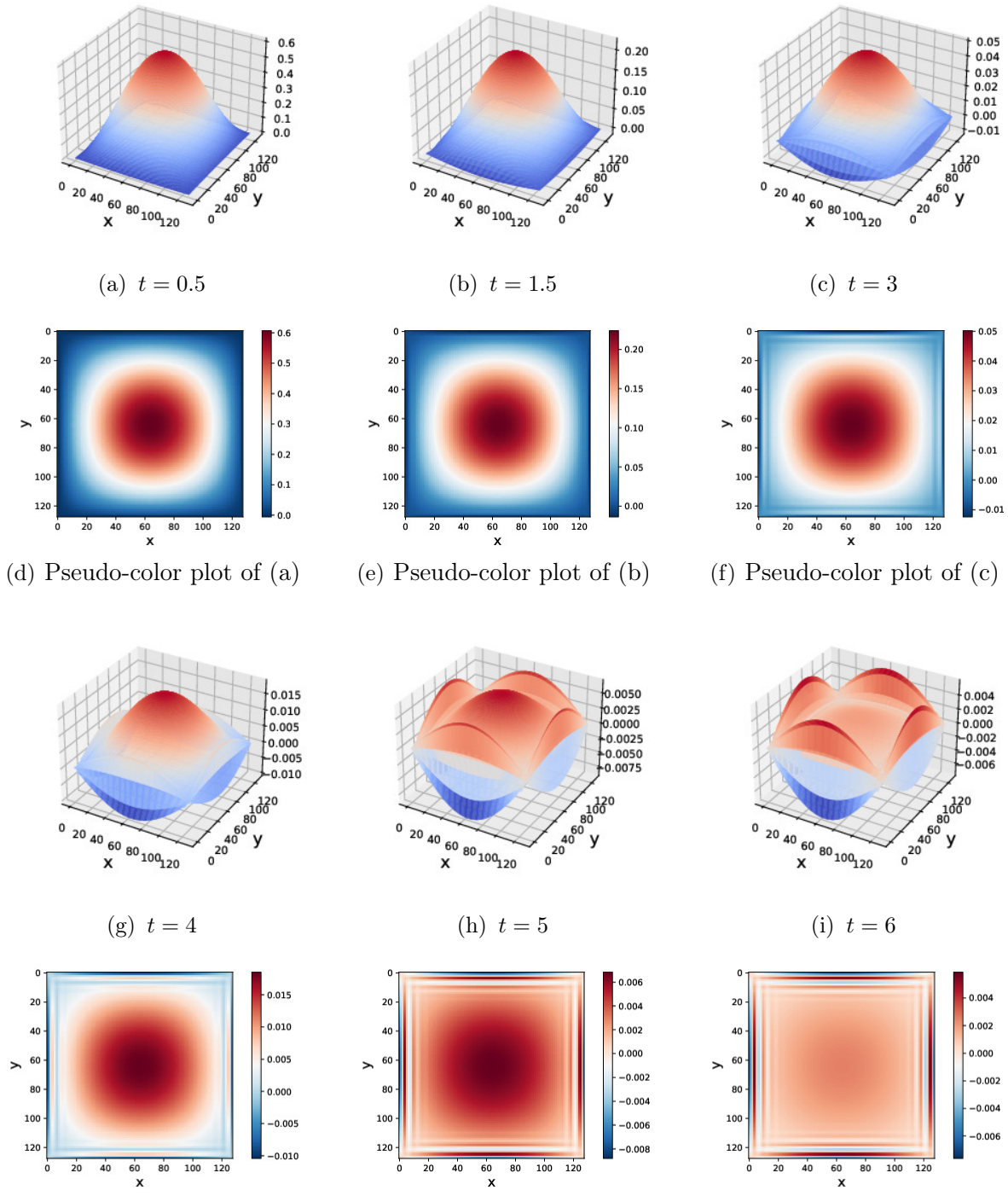

(a) $t = 0.5$ (b) $t = 1.5$ (c) $t = 3$

(d) Pseudo-color plot of (a) (e) Pseudo-color plot of (b) (f) Pseudo-color plot of (c)

(g) $t = 4$ (h) $t = 5$ (i) $t = 6$

(j) Pseudo-color plot of (g) (k) Pseudo-color plot of (h) (l) Pseudo-color plot of (i)

Fig. 5. The first and third rows are the numerical solutions of example 2 with $h = k = \dfrac{1}{128}$ and $\tau = \dfrac{4}{25}h$ at times (a) t=0.5, (b) t=1.5, (c) t=3, (g) t=4, (h) t=5, and (i) t=6. The second and fourth rows are the pseudo-color plots of the first and third rows on a uniform 128×128 mesh

The L^2 error and convergence rate of the results of example 2 at times $t = 0.5, 1.5, 3, 5$ with steps $h = k = \left\{\frac{1}{16}, \frac{1}{32}, \frac{1}{64}, \frac{1}{128}\right\}$ and $\tau = \frac{4}{25}h$ are presented in Table 3. Similarly, the dashed line in Fig. 4 confirms the decrease in mass condition of the numerical solution obtained by the proposed method for this example.

Table 2. The L^2 error of example 1 with $h = k = \frac{1}{N}$ and $\tau = \frac{4}{25}h$ at times $t = 0.5, 1.5, 3$ and $t = 5$

$h = k$	L_2-error	L_2-error [11]
1/10	9.3614e-04	9.1972e-04
1/20	2.1364e-04	2.3743e-04
1/40	2.2245e-04	2.1476e-04

Table 3. L^2 error of example 2 with $h = k = \frac{1}{N}$ and $\tau = \frac{4}{25}h$ at times $t = 0.5, 1.5, 3$ and $t = 5$

N	$t = 0.5$	order	$t = 1.5$	order	$t = 3$	order	$t = 5$	order
16	3.8496e-02	–	5.2156e-02	–	5.7316e-02	–	8.0701e-02	–
32	1.4997e-02	1.36	1.9222e-02	1.44	1.7397e-02	1.72	2.3202e-02	1.80
64	4.2471e-03	1.82	4.9415e-03	1.96	6.4727e-03	2.15	5.0142e-03	2.21
128	9.6364e-04	2.14	1.0339e-03	2.25	1.1674e-03	2.47	1.0181e-03	2.30

Example 3. In the last example, we simulate spinodal decomposition, energy dissipation, and mass conservation. We consider the Sivashinsky equation (1) with respect to the following random (normal distribution) initial value:

$$u_0(x, y) = 0.5 + \sigma \text{randn}(x, y), \quad (x, y) \in \Omega = [0, 1] \times [0, 1], \tag{32}$$

with the mean deviation $\sigma = 0.5$ and the standard deviation $\sigma = 0.25$. Binary alloy solidification with random initial conditions is used to study how microscopic fluctuations evolve into macroscopic solidification patterns. Similar to the above examples, the numerical profiles of this example with steps sizes $h = k = \frac{1}{128}$ and $\tau = \frac{4}{25}h$ at times $t = \{3, 10, 20, 40, 80, 120\}$ are shown in Fig. 6.

The L^2 errors, including the convergence rate of the numerical results of example 3 at times $t = 0.5, 1.5, 3, 5$ with steps $h = k = \left\{\frac{1}{16}, \frac{1}{32}, \frac{1}{64}, \frac{1}{128}\right\}$ and $\tau = \frac{4}{25}h$, are given in Table 4. The dotted line in Fig. 4 also shows the decrease in mass of the proposed scheme for example 3.

Table 4. L^2 error of example 3 with $h = k = \frac{1}{N}$ and $\tau = \frac{4}{25}h$ at times $t = 0.5, 1.5, 3$ and $t = 5$

N	$t = 0.5$	order	$t = 1.5$	order	$t = 3$	order	$t = 5$	order
16	4.3364e-02	–	3.0082e-02	–	2.3488e-02	–	1.8926e-02	–
32	2.7793e-02	0.64	1.9014e-02	0.66	1.4676e-02	0.68	1.2242e-02	0.63
64	1.1613e-02	1.26	8.3152e-03	1.19	6.9209e-03	1.08	6.1555e-03	0.99
128	2.4584e-03	2.24	1.8479e-03	2.17	1.5921e-03	2.12	1.4457e-03	2.09

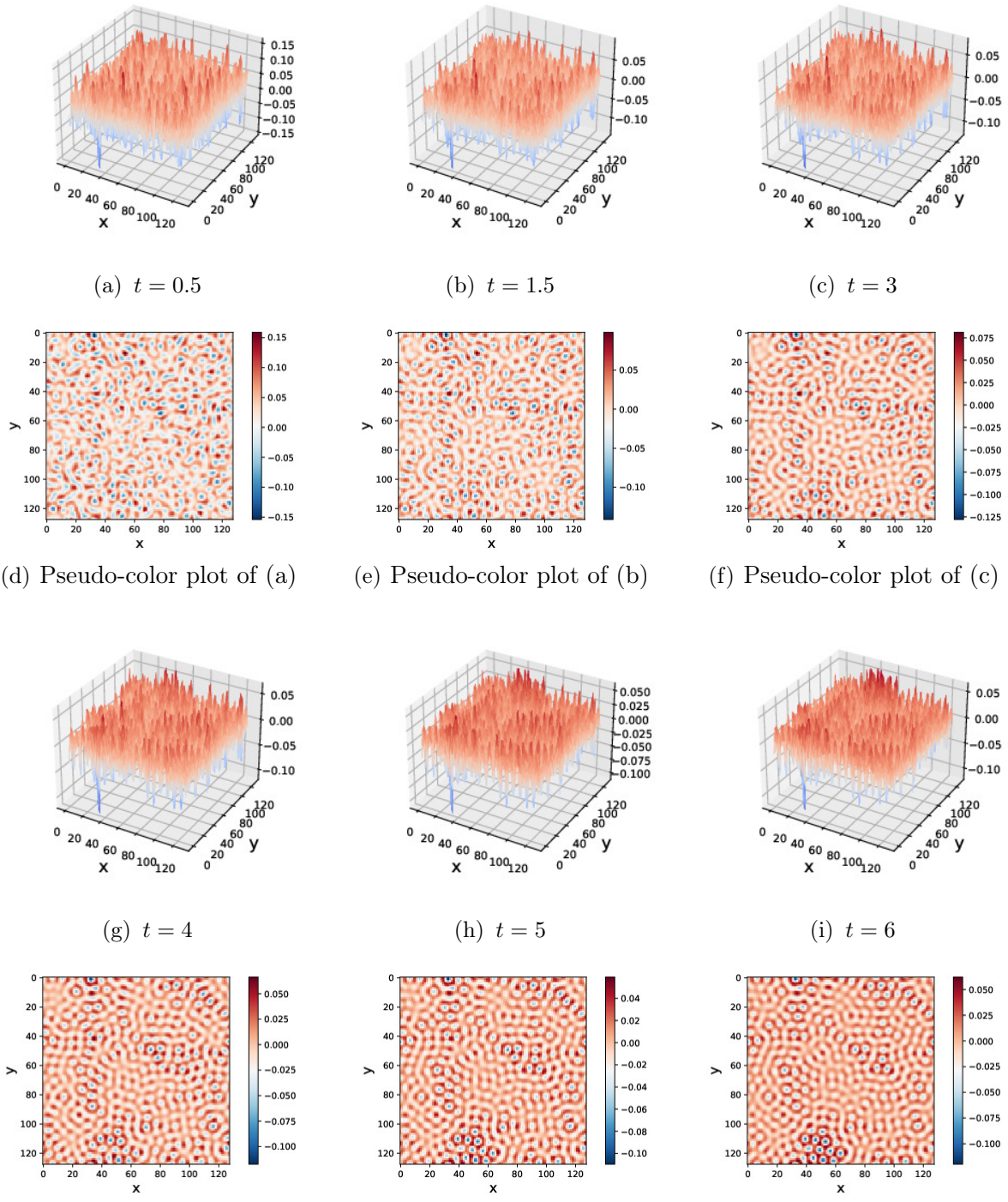

(a) $t = 0.5$ (b) $t = 1.5$ (c) $t = 3$

(d) Pseudo-color plot of (a) (e) Pseudo-color plot of (b) (f) Pseudo-color plot of (c)

(g) $t = 4$ (h) $t = 5$ (i) $t = 6$

(j) Pseudo-color plot of (g) (k) Pseudo-color plot of (h) (l) Pseudo-color plot of (i)

Fig. 6. The first and third rows are the numerical solutions of example 3 with $h = k = \dfrac{1}{128}$ and $\tau = \dfrac{4}{25}h$ at times (a) t=3, (b) t=10, (c) t=20, (g) t=40, (h) t=80, and (i) t=120. The second and fourth rows are the pseudo-color plots of the first and third rows on a uniform 128×128 mesh

Remark 3. The numerical profiles of examples 1, 2, and 3 with the same initial values as in (30), (31), and (32) are listed in Figs. 7, 8, and 9, respectively, but for $\alpha = 0.5$. A comparison of the results for $\alpha = 1$ and $\alpha = 0.5$ reveals that a decrease in the positive constant α causes the numerical solutions to tend rapidly towards the equilibrium state.

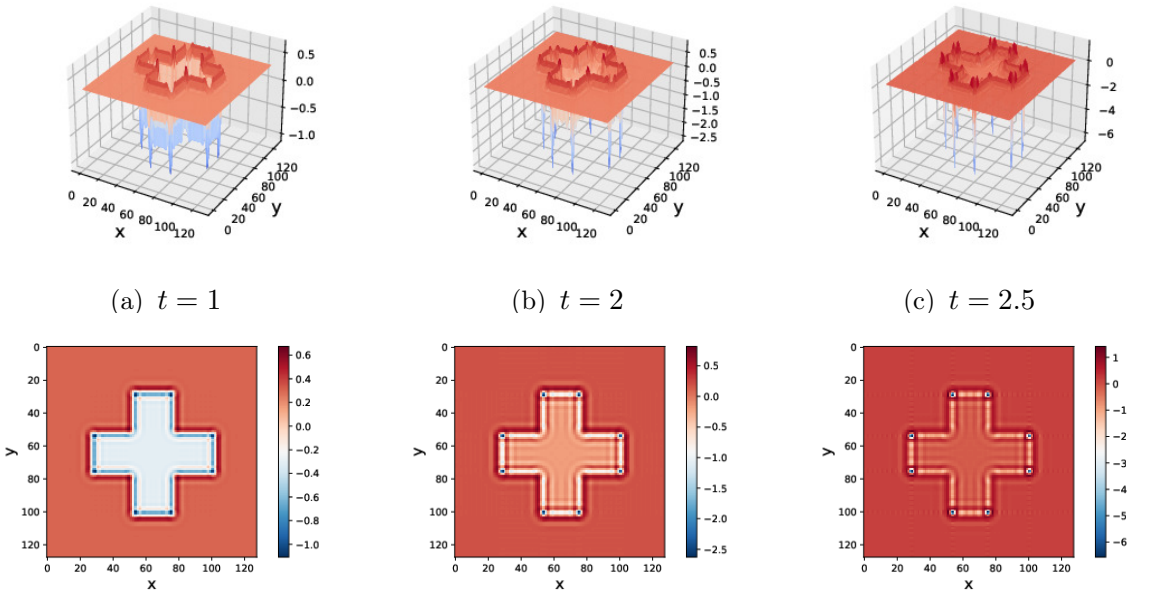

(a) $t = 1$ (b) $t = 2$ (c) $t = 2.5$

(d) Pseudo-color plot of (a) (e) Pseudo-color plot of (b) (f) Pseudo-color plot of (c)

Fig. 7. Numerical profile of example 1 for $\alpha = 0.5$, (a) $t = 1$, (b) $t = 2$, and (c) $t = 2.5$. Panels (d), (e), and (f) are the pseudo-color plots of (a), (b), and (c), respectively, on a uniform 128×128 mesh

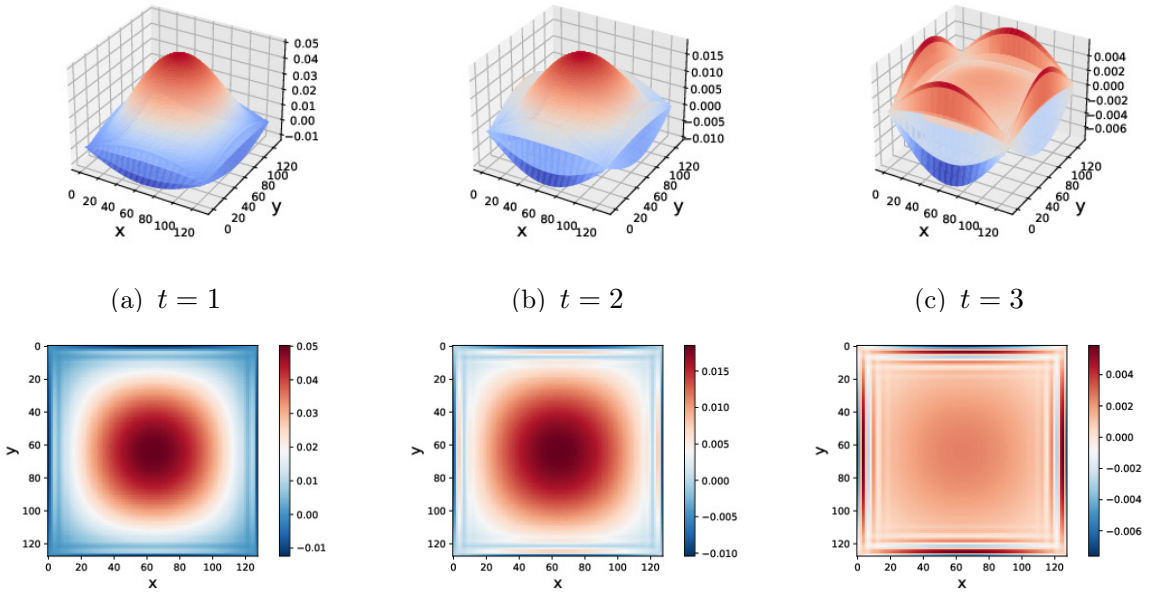

(a) $t = 1$ (b) $t = 2$ (c) $t = 3$

(d) Pseudo-color plot of (a) (e) Pseudo-color plot of (a) (f) Pseudo-color plot of (a)

Fig. 8. Numerical profile of example 2 for $\alpha = 0.5$, (a) $t = 1$, (b) $t = 2$, and (c) $t = 3$. Panels (d), (e), and (f) are the pseudo-color plots of (a), (b), and (c), respectively, on a uniform 128×128 mesh

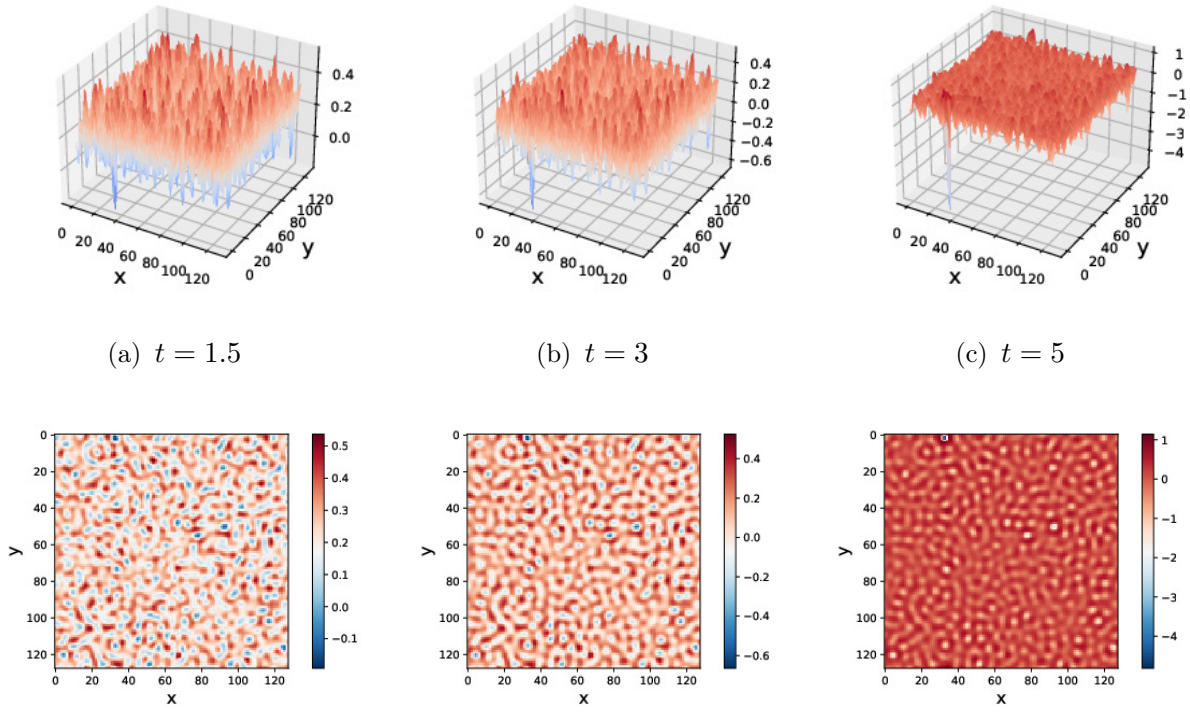

(a) $t = 1.5$ (b) $t = 3$ (c) $t = 5$

(d) Pseudo-color plot of (a) (e) Pseudo-color plot of (b) (f) Pseudo-color plot of (c)

Fig. 9. Numerical profile of example 3 for $\alpha = 0.5$, (a) $t = 1.5$, (b) $t = 3$, and (c) $t = 5$. Panels (d), (e), and (f) are the pseudo-color plots of (a), (b), and (c), respectively, on a uniform 128×128 mesh

5. Conclusions

In this article, the 2D Sivashinsky equation was studied numerically as a mathematical model for a planar solid–liquid interface dynamics in a binary alloy that naturally arises in material sciences. The mathematical formulation of this model is a fourth-order nonlinear partial differential equation for which no analytical solution exists, except for trivial solutions. The Fourier spectral method combined with the Euler method was proposed to approximate the solution of the governing equation with periodic boundary conditions. It was proved theoretically that the numerical solutions obtained by the proposed approach preserve the decreasing of mass property. Three examples (with a benchmark cross initial value, with a smooth initial value, and with a random initial value) were analyzed to validate the performance of the introduced scheme. A custom Python code was developed to solve numerically the selected examples. The accuracy of the method was assessed in the L_2 error norm. Based on the obtained numerical results, the following conclusions were reached:

- The numerical experiments confirm that the theoretical results are in good agreement with previously published data.
- With an increase in time, the numerical mass of the solutions decreased in all examples, and the obtained numerical solutions tend to a steady state.
- Figs. 3, 5, and 6 demonstrate that, for a smooth initial value, as time increased, the coarsening process led to a sample with separated regions of the blue and red phases.

Conflicts of Interest. The author declares no conflicts of interest.

Конфликт интересов. Автор заявляет об отсутствии конфликта интересов.

References

1. Caroli B., Caroli C., Roulet B. The Mullins-Sekerka instability in directional solidification of thin samples. *J. Cryst. Growth*, 1986, vol. 76, no. 1, pp. 31–49. https://doi.org/10.1016/0022-0248(86)90006-0.

2. Karma A., Rappel W.-J. Quantitative phase-field modeling of dendritic growth in two and three dimensions. *Phys. Rev. E*, 1998, vol. 57, no. 4, pp. 4323–4349. https://doi.org/10.1103/PhysRevE.57.4323.

3. Dantzig J.A., Rappaz M. *Solidification*. Ser.: Materials. Engineering Sciences. Boca Raton, FL, EPFL Press, 2009. 621 p.

4. Das A., Mittemeijer E.J. Simulation of solidification structures of binary alloys. *Z. Metallkd.*, 2002, vol. 93, no. 5, pp. 459–467. http://dx.doi.org/10.3139/146.020459.

5. Rappaz M. et al. Solute redistribution during solidification: Principles and applications. *J. Mater. Sci.*, 2008, vol. 43, no. 15, pp. 4890–4899.

6. Liotti E., Arteta C., Zisserman A., Lui A., Lempitsky V., Grant P.S. Crystal nucleation in metallic alloys using x-ray radiography and machine learning. *Sci. Adv.*, 2018, vol. 4, no. 4, art. eaar4004. https://doi.org/10.1126/sciadv.aar4004.

7. Sivashinsky G.I. On cellular instability in the solidification of a dilute binary alloy. *Phys. D*, 1983, vol. 8, nos. 1–2, pp. 243–248. https://doi.org/10.1016/0167-2789(83)90321-4.

8. Gertsberg V.L., Sivashinsky G.I. Large cells in nonlinear Rayleigh-Bénard convection. *Prog. Theor. Phys.*, 1981, vol. 66, no. 4, pp. 1219–1229. https://doi.org/10.1143/PTP.66.1219.

9. Sharma N., Sharma S. An efficient off-step exponential spline technique to solve Kuramoto–Sivashinsky and extended Fisher–Kolmogorov equations. *Int. J. Comput. Methods*, 2025, vol. 22, no. 5, art. 2450078. https://doi.org/10.1142/S0219876224500786.

10. Abazari R., Yildirim K. Numerical study of Sivashinsky equation using a splitting scheme based on Crank-Nicolson method. *Math. Methods Appl. Sci.*, 2019, vol. 42, no. 16, pp. 5509–5521. https://doi.org/10.1002/mma.5454.

11. Ilati M., Dehghan M. Error analysis of a meshless weak form method based on radial point interpolation technique for Sivashinsky equation arising in the alloy solidification problem. *J. Comput. Appl. Math.*, 2018, vol. 327, pp. 314–324. https://doi.org/10.1016/j.cam.2017.06.022.

12. Omrani K. A second-order splitting method for a finite difference scheme for the Sivashinsky equation. *Appl. Math. Lett.*, 2003, vol. 16, no. 3, pp. 441–445. https://doi.org/10.1016/S0893-9659(03)80070-8.

13. Omrani K., Ben Mohamed M.L. A linearized difference scheme for the Sivashinsky equation. *Far East J. Appl. Math.*, 2005, vol. 20, no. 2, pp. 179–188.

14. Benammou S., Omrani K. A finite element method for the Sivashinsky equation. *J. Comput. Appl. Math.*, 2002, vol. 142, no. 2, pp. 419–431. https://doi.org/10.1016/S0377-0427(01)00370-3.

15. Omrani K. Numerical methods and error analysis for the nonlinear Sivashinsky equation. *Appl. Math. Comput.*, 2007, vol. 189, no. 1, pp. 949–962. https://doi.org/10.1016/j.amc.2006.11.169.

16. Rouis M., Omrani K. On the numerical solution of two dimensional model of an alloy solidification problem. *Model. Numer. Simul. Mater. Sci.*, 2016, vol. 6, no. 1, pp. 1–9. http://dx.doi.org/10.4236/mnsms.2016.61001.

17. Abazari R., Rezazadeh H., Akinyemi L., Inc M. Numerical simulation of a binary alloy of 2D Cahn–Hilliard model for phase separation. *Comput. Appl. Math.*, 2022, vol. 41, no. 8, art. 389. https://doi.org/10.1007/s40314-022-02109-5.

18. Abazari R., Yildirim K. Numerical study of the 2D Cahn–Hilliard model of phase separation with logarithmic potential. *Prik. Mekh. Tekh. Fiz.*, 2025, no. 2 (390), pp. 73–95. https://doi.org/10.15372/PMTF202315360.

19. Rai N., Mondal S. Spectral methods to solve nonlinear problems: A review. *Partial Differ. Equations Appl. Math.*, 2021, vol. 4, art. 100043. https://doi.org/10.1016/j.padiff.2021.100043.

20. Moumni M., Douiri S.M., Kim J.S. Fourier-spectral method for the Landau–Lifshitz–Gilbert equation in micromagnetism. *Results Appl. Math.*, 2023, vol. 19, art. 100380. https://doi.org/10.1016/j.rinam.2023.100380.

21. Khader M.M., Tedjani A.H. Numerical simulation for the fractional-order smoking model using a spectral collocation method based on the Gegenbauer wavelet polynomials. *J. Appl. Anal. Comput.*, 2024, vol. 14, no. 2, pp. 847–863. https://doi.org/10.11948/20230178.

Author Information

Reza Abazari, PhD, Assistant Professor, Department of Mathematics, University of Mohaghegh Ardabili

E-mail: *abazari-r@uma.ac.ir*

ORCID: https://orcid.org/0000-0003-0125-2958

Kenan Yildirim, PhD, Professor, Faculty of Mathematics, Muş Alparslan University

E-mail: *k.yildirim@alparslan.edu.tr*

ORCID: https://orcid.org/0000-0002-4471-3964

Информация об авторах

Реза Абазари, PhD, ассистент-профессор, кафедра математики, Университет Мохагеха Ардебили

E-mail: *abazari-r@uma.ac.ir*

ORCID: https://orcid.org/0000-0003-0125-2958

Кенан Йилдирим, PhD, профессор, факультет математики, Университет Муш Альпарслан

E-mail: *k.yildirim@alparslan.edu.tr*

ORCID: https://orcid.org/0000-0002-4471-3964

Received March 25, 2025 Поступила в редакцию 25.03.2025

Accepted September 22, 2025 Принята к публикации 22.09.2025